Available online at website: https://journal.bcrec.id/index.php/bcrec

Bulletin of Chemical Reaction Engineering & Catalysis, 21 (4) 2026, xxx-xxx

Original Research Article

Stacking-Order-Dependent Interfacial Synergy in ZnO/SnO_2 and SnO_2/ZnO Heterostructured Nanofilms for Enhanced Photocatalytic, Sonocatalytic, and Antibacterial Activities

Mohamed Amine Bezzerrouk[1,*], Ahmed Akriche[1,2], Bachir Kharroubi[1], Ismail Hattabi[1], Fabien Giovannelli[3], Bruno Pignon3, Rabie Naceur[1], Mohamed Bousmaha[1,*]

[1]Research Laboratory of Industrial Technologies, Faculty of Applied Sciences, University of Tiaret, Algeria
[2]University of Kasdi Merbah Ouargla, BP 511, Ouargla, 30000, Algeria
[3]GREMAN UMR 7347, CNRS, University of Tours, INSA Centre Val de Loire, Tours, France.

Received: 13th July 2026; Revised: 8th September 2026; Accepted: 10th September 2026
Available online: 25th September 2026; Published regularly: December 2026

Abstract

In this work, ZnO/SnO_2 and SnO_2/ZnO composite thin films were synthesized by ultrasonic spray pyrolysis technique on silicon and glass substrates to investigate the effect of stacking order on structural, optical and catalytic properties. X-ray diffraction confirmed the existence of both hexagonal wurtzite ZnO and tetragonal rutile SnO_2 phases with no detectable secondary phases confirming the high performance of the deposition technique. SEM analysis revealed a dense and homogeneous surface composed of compact nanoscale grains, while EDX confirmed high chemical purity. Optical measurements exhibited an average transmittance value of ~75% for ZnO/SnO_2 and ~80% for SnO_2/ZnO thin films in the visible region. Photocatalytic and sonocatalytic activities were evaluated through the degradation of the methylene blue dye. ZnO/SnO_2 composite thin films exhibited enhanced photocatalytic efficiency, whilst SnO_2/ZnO structures displayed higher sonocatalytic peformance, highlighting the remarkable effect of the deposition sequence on the catalytic behavior. In addition, the composites exhibited strong antibacterial activity against *Pseudomonas* bacteria. The ZnO/SnO_2 configuration, with ZnO in contact with the agar exhibits markedly stronger antibacterial activity, as evidenced by a significant decrease in bacterial proliferation, compared to the relatively lower activity observed for the SnO_2/ZnO configuration. Multiple mechanisms are responsible for this effect, including oxygen vacancies and surface electronic states, which can promote electron transfer to dissolved oxygen even under dark conditions. These findings highlight the strong influence of stacking order of ZnO/SnO_2 and SnO_2/ZnO systems for various applications, including sonocatalysis, photocatalysis and antibacterial activity.

Keywords: ZnO/SnO_2; SnO_2/ZnO; Sonocatalysis; Photocatalysis; Antibacterial

How to Cite: Bezzerrouk, M. A., Akriche, A., Kharroubi, B., Hattabi, I., Giovannelli, F., Pignon, B., Naceur, R., Bousmaha, M. (2026). Stacking-Order-Dependent Interfacial Synergy in ZnO/SnO_2 and SnO_2/ZnO Heterostructured Nanofilms for Enhanced Photocatalytic, Sonocatalytic and Antibacterial Activities. *Bulletin of Chemical Reaction Engineering & Catalysis*, 21 (4), xxx-xxx. (DOI: 10.9767/bcrec.20794)

Permalink/DOI: https://doi.org/10.9767/bcrec.20794

1. Introduction

The continuously escalating global water crisis, caused by industrial effluents and organic pollutants, remains a critical challenge for global water security and environmental sustainability. Photocatalysis and sonocatalysis as advanced oxidation processes have gained significant traction thanks to their ability to degrade dyes into harmless products. Zinc oxide (ZnO) and Tin oxide (SnO_2) semiconductors are among the best choice due to their attractive physical and chemical properties and their potential applications in various fields. These materials are widely used in photocatalytic application due to their non-toxicity, eco-friendly characteristics and excellent catalytic activity [1-8]. Various techniques for synthesizing these materials such

* Corresponding Authors.
Email: mohamed.bousmaha@univ-tiaret.dz (M. Bousmaha)
mabezzerrouk@univ-tiaret.dz (M.A. Bezzerrouk)

as spray pyrolysis [9-11], hydrothermal methods [12], Sol gel [13] have been reported. Among these techniques, spray pyrolysis as a simple, cost-effective process, is vastly used to synthesized pure and doped metal oxide thin films [14-19]. However, the efficiency of single-layer films is limited by the rapid recombination of generated electron-hole (e^-, h^+) pairs. Owing to the synergetic interactions between different metal element, mixed metal oxides exhibit a higher density of active sites, enhanced stability, and high electrical conductivity compared to their single-metal oxide counterpart [20-21]. Recent research has focused on the architectural structure of heterojunctions, where the stacking order determines the catalytic pathway. Mixed ZnO-SnO_2 thin films fabricated via RF magnetron sputtering from powder targets at different durations deposition. The results indicated that the ZnO-SnO_2 as photocatalysts can effectively degrade dye pollutants under sunlight irradiation without posing any harmful effects on aquatic organisms, the authors reported that ZnO-SnO_2 film deposited for 1 h exhibited the highest photocatalytic activity. This improvement was mainly related to enhanced charge carrier mobility and concentration, together with the presence of intrinsic defects such as oxygen vacancies that facilitate interfacial charge transfer. These defects play the role of electron trapping centres, reducing electron-hole recombination.

Furthermore, the synergetic interaction at the ZnO/SnO_2 interface improves adsorption properties and promotes extende charge separation through efficient interfacial charge transfer between the two semiconductor components [22,23]. An enhanced photocatalytic efficieny was in the SnO_2/ZnO/TiO_2 thin film heterostructure relative to single-component films, owing to its heterostructural design, which promotes efficient charge separation, reduces electron-hole recombination and increases the avaibility of charge carriers for photo-degradation reaction [24]. $BaTiO_3$/ZnO heterostructured photocatalyst was used to decompose the methylene blue under UV irradiation, Approximately, 94% of methylene blue was degraded within 60 min, which is attributed to the enhanced charge carrier separation arising from the heterojunction interface [25]. In another investigation [26], A ZnO/SnO_2 heterostructure consisting of ZnO nanorods decorated with SnO_2 nanoparticles were fabricated on glass fiber membranes. The sample with a 40% surface coverage exhibited the highest photocatalytic performance toward methylene blue degradation. ZnO/SnO_2 heterostructure exhibits the highest degradation of 82.45% compared to the individual components, pure ZnO (38.55%) and SnO_2 (32.68%) under visible light illumination for 2 hours. This improved photo-degradation arises from the efficient separation of charge carriers and interfacial interactions within the novel heterostructure [27]. SnO_2/ZnO films were employed as photocatalysts in hygrogen production. Under UV light irradiation, a hydrogen yields up to 70 μmol was achieved after 3 hours in the first experiment. In contrast, the photocatalytic activity declined markedly during the second cycle due to the photocorrosion of the films [28]. This phenomenon can be attributed to the photogenerated holes produced during the activation of the photocatalyst [29]. The photocatalytic performance of ZnO-SnO_2 nanocomposites synthesized via sol-gel method [30] and chemical precipitation techniques [31] was systematically investigated.

ZnO/SnO_2 nanocomposites with varying SnO_2 contents were prepared using sol-gel technique to study changes in the electrical properties at room temperature and low temperatures [32], the increased impedance observed at low temperatures resulted from their semiconducting behaviour and limited thermal energy of charge carriers. In another research, when SnO_2/ZnO and Fe-doped SnO_2/ZnO heterostructures were prepared using hydrothermal method to evaluate their gas-sensing characteristics [33]. An improved xylene response was observed due to the porous nature in the nanoplatelets of Fe/SnO_2/ZnO, which increased gas adsorption. Based on these studies, the efficiency of individual component is constrained by the rapid recombination of photo-generated electro-hole pairs. In response to this challenge, ZnO/SnO_2 and SnO_2/ZnO composite nanofilms were prepared via ultrasonic spray pyrolysis technique. The synthesized composites were systematically investigated as sonocatalysts and photocatalysts for methylene blue (MB) degradation, as well as for antibacterial activity against *Pseudomonas* bacteria. The novelty of this work lies in demonstrating that the deposition sequence of ZnO/SnO_2 and SnO_2/ZnO heterostructures significantly influences their photocatalytic, sonocatalytic and antibacterial performances, offering new insights into the strategic design of multi-layered thin films for hybrid water treatment and antimicrobial disinfection technologies.

2. Materials and Methods

2.1. Preparation of Composite Thin Films

ZnO/SnO_2 and SnO_2/ZnO composite thin films were fabricated via ultrasonic spray pyrolysis (Figure 1). A glass and silicon substrates were used for characterization as well as on glass tubes for the dye degradation studies. The substrates were kept on the hotplate during deposition with

temperature of 350 °C for ZnO and 450 °C for SnO_2. The precursor solutions were prepared by dissolving zinc acetate dehydrated ($Zn(CH_3COO)_2{\cdot}2H_2O$) in methanol ($CH_3OH$) and Tin(II) chloride dehydrate ($SnCl_2.2H_2O$) in ethanol (C_2H_5OH), each at a molar concentration of 0.3 M. The solutions were stirred at 40 °C for 30 min and subsequently heated at 60 °C for 2 h to obtain homogeneous mixtures. Air was employed as the carrier gas at a controlled flow rate of 0.5 L/min to convey the aerosol generated by an ultrasonic transducer operating at a frequency of 40 kHz toward the heated substrate. To obtain the composite structure, SnO_2 was first deposited on the substrate, followed by the deposition of ZnO thin film on the top of the SnO_2 thin film to form ZnO/SnO_2 composite thin film. Subsequently, ZnO was deposited on the substrate, and a SnO_2 thin film was then deposited on the top of the ZnO thin film, resulting in SnO_2/ZnO composite thin film.

2.2. Characterization Methods

The structural properties of the synthesized composites were analyzed by X-ray diffraction (XRD) using a BRUKER D8 ADVANCE diffractometer with Cu-Kλ radiation ((λ = 0.15418 nm), operated at 40 kV and 40 mA. The diffraction patterns were collected over 2θ range of 20-70°. The surface morphology, microstructure, and elemental composition of the composites thin films were investigated by scanning electron microscopy coupled with energy-dispersive X-ray spectroscopy (SEM-EDX, Tescan MIRA3). Transmission spectra were recorded using aUV-Visible spectrophotometer (JASCO V-630), which was also employed to monitor methylene blue degradation during the photocatalytic and sonocatalytic experiments.

2.3. Photocatalytic and Sonocatalytic Activities

Photocatalytic and sonocatalytic activities of ZnO/SnO_2 and SnO_2/ZnO composite thin films were controlled by the degradation of methylene blue with concentration of 5 mg/L under Ultraviolet (UV) and Ultrasonic (US) irradiations, respectively. To increase the interfacial contact between catalyst and the methylene blue dye solution, the thin films were coated onto the inner surface of a transparent glass tube. The photo-degradation and sono-degradation efficiencies (D_{PS} %) were calculated using Equation (1):

$$D_{PS}(\%) = \frac{C_0 - C_t}{C_0}.100\% \quad (1)$$

Where C_0 represent the initial concentration of MB and C_t corresponds to the concentration at a given time t.

2.4. Antibacterial Activity

The antibacterial activity of the synthesized ZnO/SnO_2 and SnO_2/ZnO thin films was examined using Mueller-Hinton Agar disc diffusion technique against *Pseudomonans aeruginosa*. The bacterial suspension was calibrated to a 0.5 McFarland turbidity equivalent to 10^8 colony-forming units (CFU/mL). The bacterial solution was the diluted to be equivalent to 10^6 CFU/mL. After culture, the bacterial solution was diffused onto a nutrient agar plate at 37 °C for overnight.

3. Results and Discussion

3.1. X-ray Diffraction

Figure 2 displays the XRD patterns of both ZnO/SnO_2 and SnO_2/ZnO composite oxide thin films, revealing their microstructural properties.

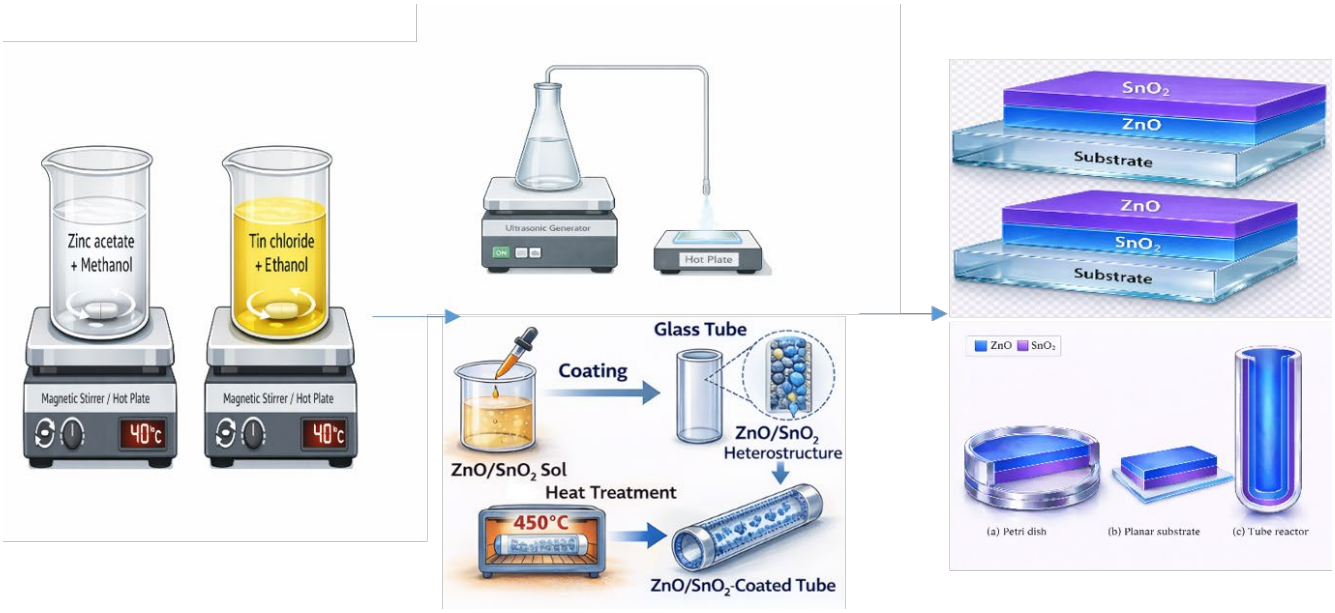

Figure 1. Schematic diagram of the preparation process of ZnO/SnO_2 and SnO_2/ZnO composite thin films.

All diffraction peaks in Figure 2(a, b) confirm the coexistence of the hexagonal wurtzite structure of ZnO (JCPDS 36-1451) and the tetragonal rutile structure of SnO_2 (JCPDS 41-1445). For ZnO/SnO_2 composite thin film, the diffraction peaks at 2θ values of 31.7, 34.3, 36.2, 47.4, 56.6, 62.7, 67.9 and 68.9° are indexed to the (100), (002), (101), (102), (110), (103), (112) and (201) planes of hexagonal wurtzite ZnO. The diffraction peaks at 26.4, 33.7, 37.8, 51.5, 54.5, 64.8 and 65.6° are assigned to the (110), (101), (200), (211), (220), (310) and (301) planes of tetragonal rutile SnO_2, and for SnO_2/ZnO composite thin film, the diffraction peaks at 26.4, 33.7, 37.8, 51.5, 54.5, 64.8 and 65.6° are assigned to the (110), (101), (200), (211), (220), (310), and (301) planes of tetragonal rutile SnO_2. The diffraction peaks at 2θ values of 31.7, 34.4, 36.2, 47.4, 56.6, 62.7, 67.9 and 68.9° are indexed to the (100), (002), (101), (102), (110), (103), (112) and (201) planes of hexagonal wurtzite ZnO. These diffraction peaks confirm that both hexagonal wurtzite ZnO and tetragonal rutile SnO_2 phases coexist in the ZnO/SnO_2 and SnO_2/ZnO composite films, indicating that ZnO is successfully deposited on SnO_2 and SnO_2 is successfully deposited on ZnO. It is also noted that the characteristic SnO_2 peaks in the ZnO/SnO_2 composite and the ZnO peaks in the SnO_2/ZnO composite are still present, confirming that neither phase disappears in the heterostructures.

The structural parameters, including the lattice constants (a, c) and the (c/a) ratio, the crystallite size (D), microstrain (ε) and dislocation density (δ) were determined from the first crystallographic planes (100), (002), (101) for ZnO and (110), (101), (200) for SnO_2 using the following equations:

$$2d_{hkl}sin\theta = n\lambda \quad (2)$$

$$(\text{ZnO})\ \frac{1}{d_{hkl}^2} = \frac{4}{3}\frac{(h^2+hk+k^2)}{a^2} + \frac{l^2}{c^2} \quad (3)$$

$$(\text{SnO}_2)\ \frac{1}{d_{hkl}^2} = \frac{h^2+k^2}{a^2} + \frac{l^2}{c^2} \quad (4)$$

$$D = \frac{0.9\lambda}{\beta cos\theta} \quad (5)$$

$$\varepsilon = \frac{\beta cos\theta}{4} \quad (6)$$

$$\delta = \frac{1}{D^2} \quad (7)$$

where λ is the wavelength, β is the full width at half maximum (FWHM) of the diffraction peak and θ is the Bragg's diffraction angle. The calculated lattice parameters are listed in Table 1. These values for both ZnO and SnO_2 in the two composite configurations are in good agreement with literature values [32,34,35], thereby confirming the phase purity of the composite structures. The crystallite sizes range from 16.61 to 23.33 nm, indicating well-crystallized nanocomposite thin films suitable for enhanced photocatalytic and sonocatalytic applications.

In order to better understand the differences in crystallite sizes between the two phases in the two configurations and stacking-dependent growth, a comparative analysis is presented in Table 2. It can be observed that the crystallite size of ZnO in the ZnO/SnO_2 configuration (ZnO on top of SnO_2) is larger than that in the SnO_2/ZnO composite (ZnO beneath SnO_2). A similar trend is noted for SnO_2, whose crystallite size in the SnO_2/ZnO composite (SnO_2 on top of ZnO) is greater than that in the ZnO/SnO_2

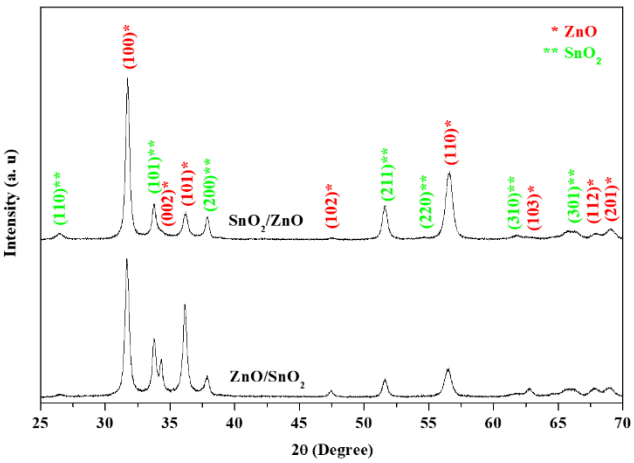

Figure 2. XRD pattern of ZnO/SnO_2 and SnO_2/ZnO composite thin films.

Table 1. Lattice parameters of ZnO and SnO_2 in ZnO/SnO_2 and SnO_2/ZnO composites.

	Composites	a (Å)	c (Å)	c/a	(h k l)	FWHM	D (nm)
ZnO	ZnO/SnO_2	3.26	5.22	1.60	(100)	0.4081	20.25
					(002)	0.3068	27.12
					(101)	0.3695	22.63
	SnO_2/ZnO					0.3800	21.75
						0.4790	17.38
						0.4460	18.75
SnO_2	SnO_2/ZnO	4.75	3.19	0.67	(110)	0.6575	12.42
					(101)	0.3524	23.57
					(200)	0.3209	26.19
	ZnO/SnO_2					0.7124	11.46
						0.3420	24.30
						0.5970	14.08

composite (SnO_2 beneath ZnO). The consistent observation that top layer phases exhibit 21-25% larger crystallite sizes than the bottom layers suggests a systematic growth behaviour dependent on deposition sequence. This enhanced crystallinity correlates with lower microstrain and dislocation density in the top layers (Table 2), indicating reduced lattice distortion during later deposition steps of ultrasonic spray pyrolysis.

3.2. SEM and EDX Analysis

The surface microstructure and morphology of ZnO/SnO_2 and SnO_2/ZnO composite thin films were characterized by scanning electron microscopy (SEM). The images in Figure 3 show that both films exhibit a dense, continuous surface composed of compact nanoscale grains, indicating good coalescence and densification of the film. The homogeneous grain size distribution, together with the low defect density and absence of visible cracks, suggests high film quality, which is beneficial for efficient charge transport in photocatalytic and sonocatalytic processes. Overall, these SEM observations confirm the formation of high-quality composite thin film. A cross-sectional SEM analysis was performed to further investigate the layered architecture of the deposited heterostructure. Figure 3(c) presents the cross-sectional SEM image of the SnO_2/ZnO heterostructure, where two distinct layers can be observed, consistent with the sequential deposition of SnO_2 and ZnO. Thickness measurements performed at different positions yielded values ranging from 0.48 to 0.63 µm for

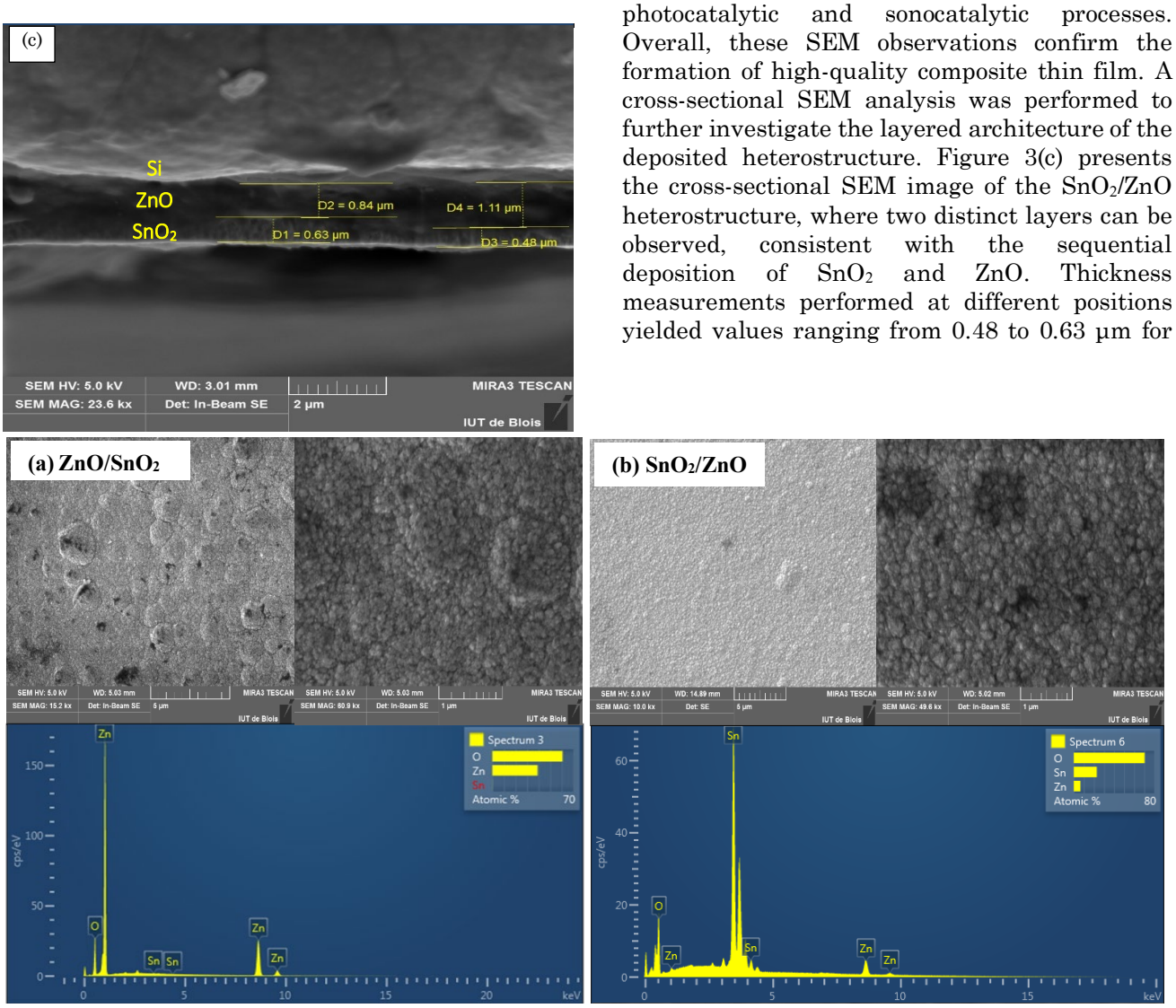

Figure 3. SEM Images with EDX analysis of ZnO/SnO_2 (a) and SnO_2/ZnO (b), Cross-Sectional SEM of SnO_2/ZnO (c).

Table 2. Comparative crystallite size, microstrain and dislocation density analysis.

Metal Oxide	Composite	Position	D_{av} (nm)	ε (%)	δ ($\times 10^{-3}$ nm^{-2})
ZnO	ZnO/SnO_2	Top	23.33	0.15	1.84
	SnO_2/ZnO	Bottom	19.29	0.18	2.68
	Difference	Top > Bottom	+4.04 (+21%)	-0.03	+0.48
SnO_2	SnO_2/ZnO	Top	20.73	0.19	2.32
	ZnO/SnO_2	Bottom	16.61	0.23	3.63
	Difference	Top > Bottom	+4.12 (+25%)	-0.04	+1.31

the SnO_2 layer and from 0.84 to 1.11 µm for the ZnO layer. Based on these measurements, the total film thickness was estimated to be approximately 1.32–1.74 µm. The clearly distinguishable layered architecture provides morphological evidence supporting the successful deposition and formation of the intended SnO_2/ZnO heterostructure.

The EDX analysis of ZnO/SnO_2 and SnO_2/ZnO composite thin films confirm the presence of the constituent elements Zn, Sn and O, with no additional impurity-related peaks within the sensitivity of the technique. In the ZnO/SnO_2 configuration a strong Zn and O peaks with low Sn intensity, consistent with a ZnO phase in the top layer and SnO_2 in the bottom layer in the composite. Conversely, in the SnO_2/ZnO configuration, the spectra are dominated by Intense Sn and O peaks with weaker Zn contribution, evidencing a SnO_2 thin film deposited on a ZnO underlayer. The corresponding atomic percentages in both composite thin films are close to the nominal stoichiometry of ZnO and SnO_2, indicating high chemical purity with absence of secondary phases or significant elemental contamination.

3.3. Optical Properties

Figure 4 displays the optical transmittance spectra in wavelength range of 350-850 nm for ZnO/SnO_2 and SnO_2/ZnO composite thin film. Both composite thin films display high transparency within the visible region. The ZnO/SnO_2 thin film exhibits an average transmittance of approximately 75%, while the SnO_2/ZnO thin film displays a higher transmittance of about 80%. In the near-ultraviolet region, both composites exhibit a sharp decrease in optical transmittance, corresponding to a strong fundamental absorption edge. This strong absorption arises from interband optical transitions of electrons from the valence band to the conduction band.

The optical band gap values of the two compounds were determined from Tauc plots using the following relationship [36]:

$$\alpha(h\upsilon) = A(h\upsilon - Eg)^{1/2} \quad (8)$$

Where α is the absorption coefficient, $h\upsilon$ is the Photon energy and Eg is the optical band gap. From the plot of $(\alpha h\upsilon)^2$ versus $(h\upsilon)$ in Figure 5, the gap energies were obtained by extrapolating the straight linear part of the curves to the photon energy axis. The ZnO/SnO_2 composite thin film exhibits a band gap of 3.24 eV, whereas the SnO_2/ZnO sample gives a slightly higher bad gap of 3.30 eV. These values correspond to absorption edges near 375-385 nm, indicating that both configurations are primarily activated under Ultraviolet or near-Ultraviolet excitation. These values are in good agreement with those reported in the literature [37-39].

3.4. Photocatalytic and Sonocatalytic Studies

Figure 6 presents the absorption spectra of Methylene blue (MB) aqueous solutions under Ultraviolet and Ultrasonic irradiations using both ZnO/SnO_2 and SnO_2/ZnO composite thin films for photocatalytic (Figure 6 (a,b)) and sonocatalytic (Figure 6 (c,d)) degradation. The visible absorption spectrum of MB exhibits a characteristic peak around 664 nm, whose intensity decreases progressively with increasing irradiation time. The ZnO/SnO_2 achieves 100% degradation after 240 min of UV irradiation and 97% degradation after 40 min of US irradiation, whereas SnO_2/ZnO reaches 65% after 240 min UV and 100% after 40 min US (Figure 7 (a,d)). Thus, the higher photocatalytic performance of ZnO/SnO_2 compared with SnO_2/ZnO is more plausibly associated with the different interfacial configurations resulting from the deposition sequence, which may influence interfacial charge transfer, defect states, crystallinity, and charge-

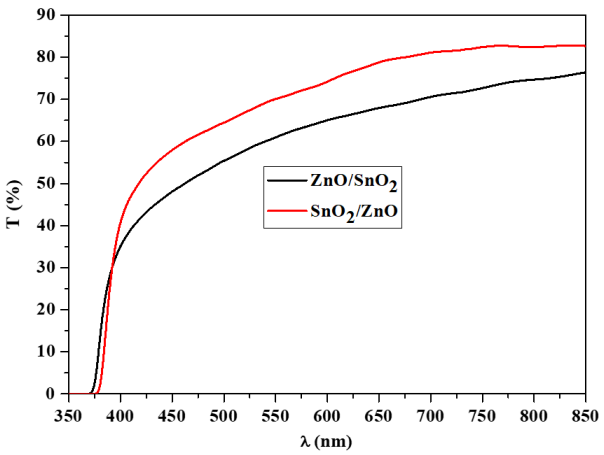

Figure 4. Transmittance spectra of ZnO/SnO_2 and SnO_2/ZnO composite thin films.

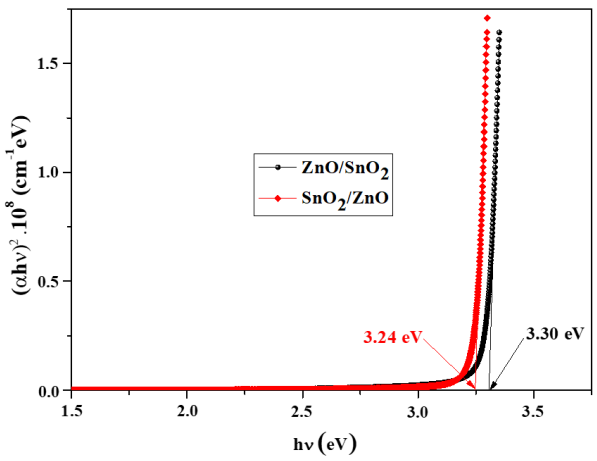

Figure 5. Tauc plot of ZnO/SnO_2 and SnO_2/ZnO composite thin films.

carrier recombination. These interfacial effects can consequently affect the availability and lifetime of photogenerated charge carriers for surface redox reactions.

In contrast, SnO_2/ZnO exhibits higher sonocatalytic activity than ZnO/SnO_2. This difference may be related, at least in part, to the distinct interfacial configuration and mechanical response of the two-layer systems under ultrasonic irradiation. The higher density of SnO_2 (6.95 g.cm^{-3}) compared with ZnO (5.6 g.cm^{-3}) may influence the mechanical behavior of the catalytic layer and its interaction with the acoustic field, although density alone cannot account for the observed difference in sonocatalytic activity. Other interfacial factors, including acoustic energy transfer, cavitation-related effects, surface properties, and charge-carrier processes, may also contribute to the enhanced sonocatalytic performance of the SnO_2/ZnO configuration [11]. In other research, High transparent ZnO-SnO_2 thin films with Zn:Sn (80:20) and sintered at 500 °C, show the higher photo-degradation against MB [40].

The contribution of direct UV photolysis to MB degradation was also investigated in our previous studies using the same irradiation conditions and in the absence of a photocatalyst [5,11]. The results showed only negligible MB degradation, confirming that direct photolysis has a limited role under the present experimental conditions. Therefore, the degradation observed in this work can mainly be attributed to the photocatalytic activity of the ZnO/SnO_2 and SnO_2/ZnO thin-film system.

The degradation processes followed pseudo-first-order kinetics, with degradation efficiencies (C/C_0) shown in Figure 7 (b,e). The rate constant k was calculated using Langmuir-Hinshelwood relation:

$$\ln\left(\frac{C}{C_0}\right) = -kt \tag{9}$$

Where k is the slope of the linear plot of $\ln(C/C_0)$ versus time presented in Figure 7 (c,f) for both photocatalysis and sonocatalysis. All correlation coefficients (R^2) exceeded the value of 0.9, confirming excellent fit to experimental data. Sonocatalysis exhibited the highest (k) values: 0.081 min^{-1} for SnO_2/ZnO and 0.073 min^{-1} for ZnO/SnO_2 composite thin films. Compared to our

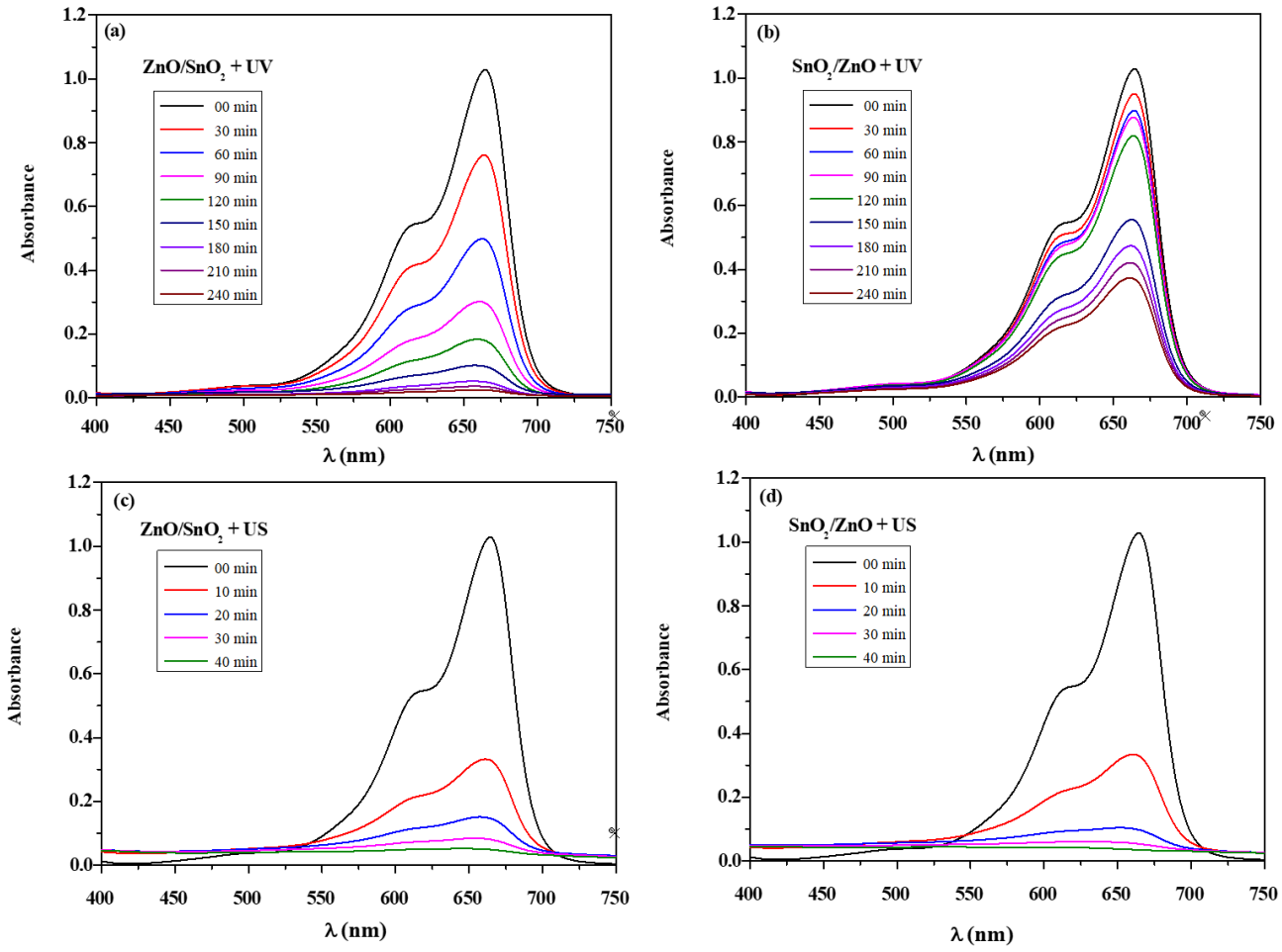

Figure 6. Absorption spectra of MB with Photocatalysis in presence of (a) ZnO/SnO_2, (b) SnO_2/ZnO and with sonocatalysis in presence of (c) ZnO/SnO_2, (d) SnO_2.

previous work on individual components, SnO_2 showed superior sonocatalytic activity with k = 0.148 min^{-1} [11]. In the other hand, for photocatalysis, ZnO/SnO_2 achieved k = 0.016 min^{-1} and SnO_2/ZnO k = 0.004 min^{-1}, both exceeding pure ZnO (k = 0.0038 min^{-1}) [24], and SnO_2 (k = 0.00055 min^{-1}, k = 0.00016 min^{-1}) [11,24]. This demonstrates the synergetic effect between ZnO and SnO_2, enhancing photo-degradation.

3.5. Photo-Sono-Degradation Mechanism

A proposed photo-sono-degradation mechanism is illustrated in Figure 8. In the photocatalytic activity when the energy of light irradiation equal or greater than the energy bandgap of the photocatalyst, electrons (e_{CB}^-) are excited in the valence band (VB) to the conduction band (CB) leaving behind a holes (h^+) [41,42]. (Equation 10). The semiconductors in the composite thin films ZnO/SnO_2 and SnO_2/ZnO exhibit matching band potentials and strong interfacial bonding. SnO_2 displays the most positive conduction band edge potential, while ZnO has the least positive valence band edge potential. This configuration enables efficient photoinduced charge transfer, with electrons and holes migrating from one semiconductor to the

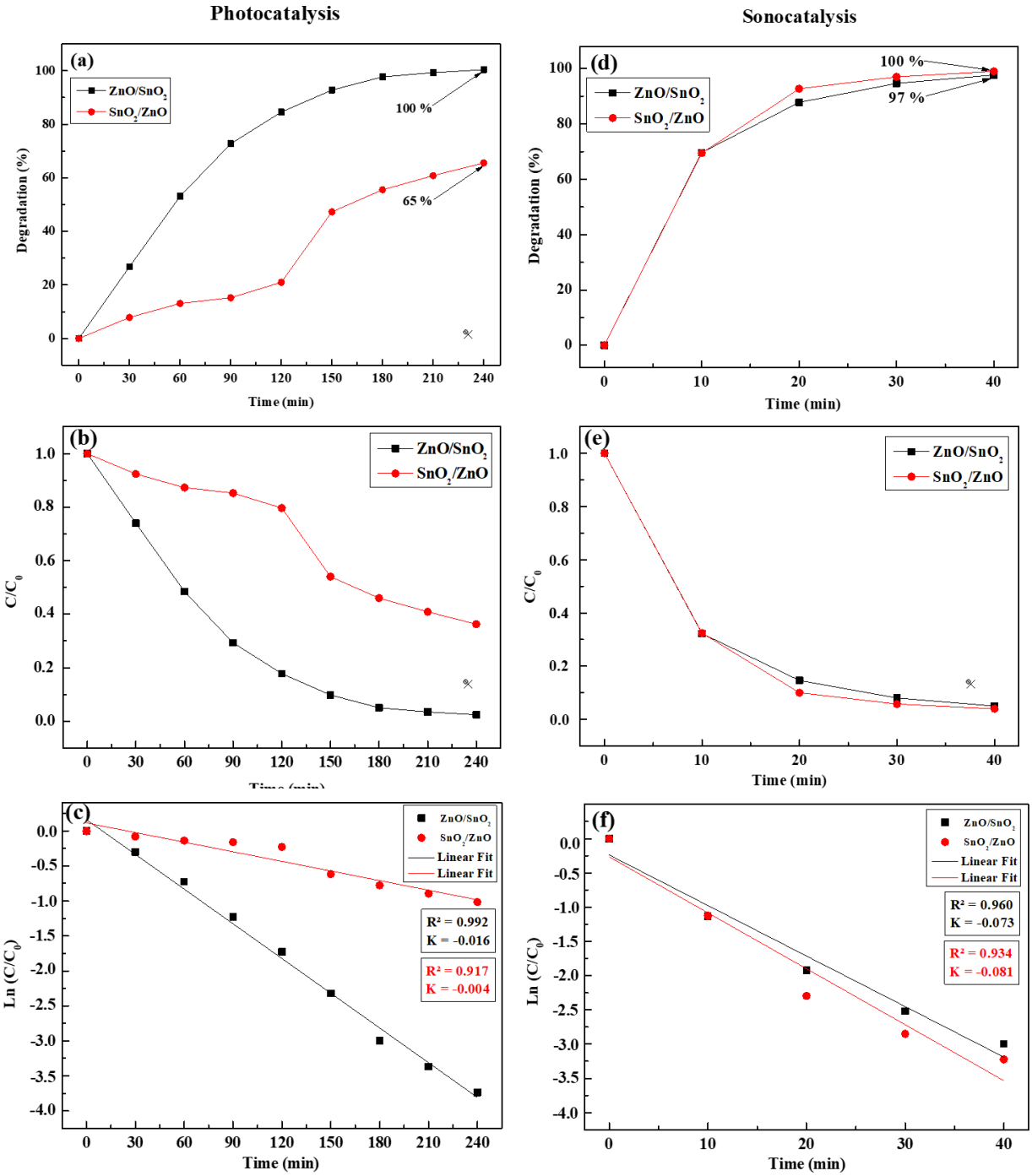

Figure 7. Degradation of methylene blue vs time, (C/C_0) vs Time (t), ln (C/C_0) vs Time (t) with photocatalysis (a,b,c) and sonocatalysis (d,e,f).

other under energy light irradiation. Under UV irradiation, the photogenerated electron-hole pairs may participate in interfacial redox reactions. The photogenerated electrons can potentially reduce dissolved oxygen molecules (O_2) to radical anion of oxygen ($\cdot O_2^-$) Equation (11), whereas photogenerated holes may oxidize surface H_2O to generate hydroxyl radicals ($\cdot OH$) Equation (12). Further reactions involving oxygen-derived species may lead to H_2O_2 formation and subsequent production of additional reactive species. These pathways represent plausible ROS-generation routes commonly proposed for semiconductor photocatalysis. In the sonocatalysis process, under US irradiation, a hot spots with high temperatures and pressure are formed by ultrasonic cavitation which pyrolyze the water molecules into ($H\cdot$) and ($\cdot OH$) radicals Equation (13).

Finally, the hydroxyl radicals and oxygen anions produced during both photocatalysis and sonocatalysis processes play a crucial role in the degradation of organic pollutants, as depicted in Equation (14).

$$ZnO/SnO_2 \text{ or } SnO_2/ZnO + h\nu \rightarrow e_{CB}^- + h_{VB}^+ \quad (10)$$

$$e_{CB}^- + O_2 \rightarrow \cdot O_2^- \quad (11)$$

$$h_{VB}^+ + H_2O \rightarrow \cdot OH + H^+ \quad (12)$$

$$ZnO/SnO_2 \text{ or } SnO_2/ZnO + US\text{ɔɔɔ} + H_2O \rightarrow H\cdot + \cdot OH \quad (13)$$

$$\cdot OH \ (or \ \cdot O_2^-) + MB\ dye \rightarrow CO_2 + H_2O + Degraded\ products \quad (14)$$

It should be noted that previous XPS investigations of ZnO and SnO_2 thin films have reported defect-related oxygen species and oxygen-vacancy-related contributions [8,11]. In ZnO thin films, the O 1s spectrum was resolved into metal-oxygen, defect-related oxygen, and organic-related contributions, with the defect-related oxygen component located at approximately 531.8 eV [8]. For SnO_2 thin films, the Sn 3d spectra revealed contributions associated with Sn^{4+} and Sn^{2+} chemical states, while the O 1s spectrum was deconvoluted into components attributed to metal-oxygen bonds, hydroxyl/defect-related oxygen species, and organic species [11]. Based on these previous reports, the possible contribution of oxygen vacancies and surface defects to the photocatalytic and antibacterial performance is therefore discussed as a plausible contributing factor rather than as a directly established mechanism.

In this study, the ZnO/SnO_2 and SnO_2/ZnO composites thin films exhibit a marked enhancement in photocatalytic and sonocatalytic performance compared to their individual components. This enhacement may be associated with improved interfacial charge-transfer processes and reduced electron-hole

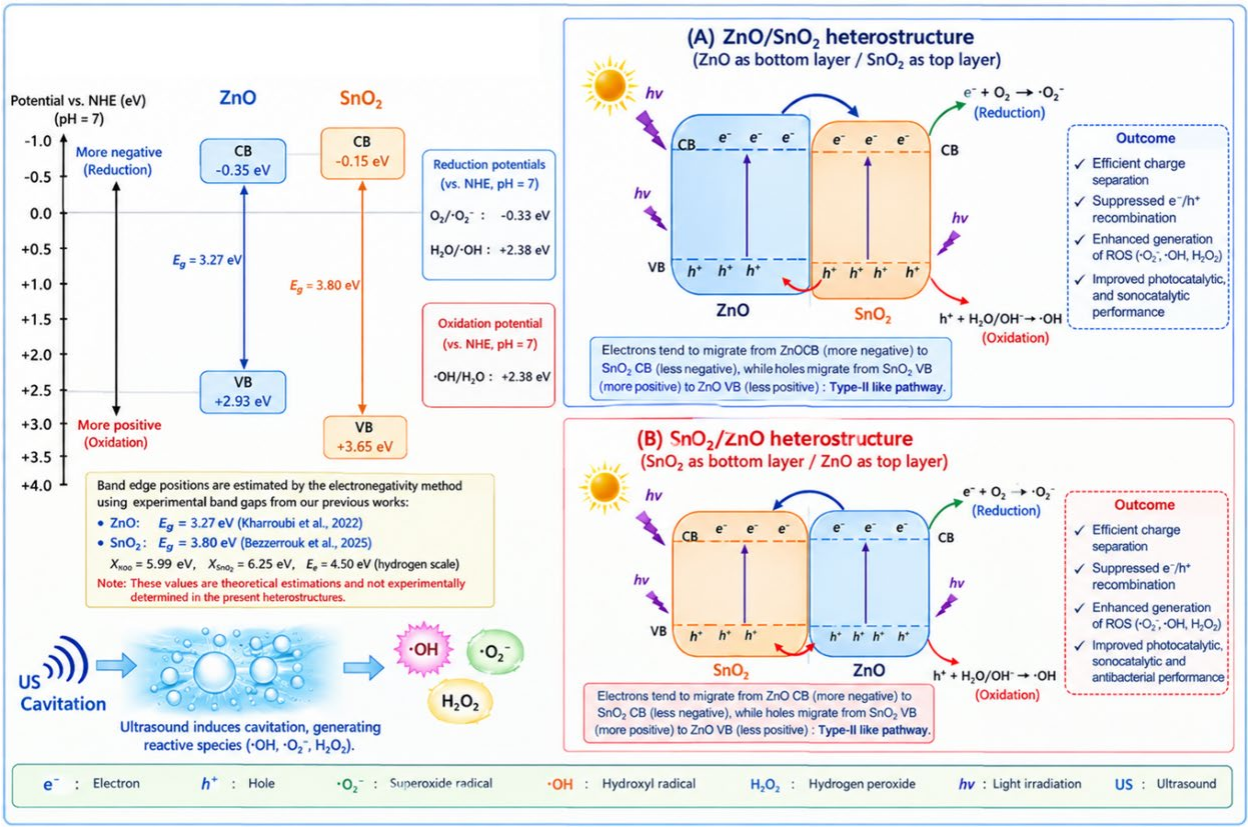

Figure 8. proposed charge transfer mechanism over ZnO/SnO_2 and SnO_2/ZnO heterostructure.

recombination at the ZnO/SnO_2 and SnO_2/ZnO heterojunction interface. These processes are proposed based on the observed photocatalytic and sonocatalytic behaviour.

3.6. Antibacterial Study

The antibacterial activity of the ZnO/SnO_2 and SnO_2/ZnO thin-film heterojunctions was qualitatively evaluated under strictly dark conditions after 24 h of incubation. The macroscopic observations presented in Figure 9(a–c) reveal clear differences in bacterial proliferation depending on the nature of the outer layer in direct contact with the agar medium. As shown in Fig. 9(a), the control sample exhibits abundant and relatively homogeneous bacterial proliferation of Pseudomonas aeruginosa, confirming that the experimental conditions and culture medium were suitable for bacterial growth and did not intrinsically inhibit proliferation. In Figure 9(b), corresponding to the SnO_2/ZnO configuration, with SnO_2 as the outer layer in contact with the agar, a noticeable reduction in bacterial proliferation is observed compared with the control, indicating a moderate antibacterial effect. In contrast, Figure 9(c), corresponding to the ZnO/SnO_2 configuration, with ZnO as the outer layer in contact with the agar, exhibits a substantially lower bacterial proliferation, suggesting a stronger antibacterial effect under the investigated dark conditions. These observations indicate that the antibacterial response is influenced by the nature of the outermost oxide layer and, consequently, by the surface properties of the heterostructure.

Since the experiments were conducted in complete darkness, the observed antibacterial activity cannot be attributed to conventional light-induced photocatalytic excitation. Instead, it may involve light-independent surface-mediated interactions between the oxide surface and bacterial cells. In the case of ZnO, previous studies have reported that oxygen vacancies and other surface electronic defects can influence charge-transfer processes involving adsorbed oxygen species, potentially contributing to the formation of reactive oxygen species (ROS) even in the absence of external illumination [43]. Such defect-mediated surface redox processes have been proposed as possible contributors to antibacterial activity under dark conditions. ROS, when generated, may induce oxidative stress through membrane lipid peroxidation, protein oxidation, and DNA damage, ultimately affecting bacterial viability [44].

However, it should be emphasized that ROS generation under dark conditions was not directly measured in the present study using specific techniques such as fluorescence-based ROS probes, electron paramagnetic resonance (EPR/ESR), or ROS-scavenging experiments. Therefore, oxygen-vacancy-mediated ROS generation is considered here as a plausible mechanistic pathway based on previous literature rather than as an experimentally demonstrated mechanism for the present ZnO/SnO_2 heterostructures. Further dedicated experiments would be required to directly verify the contribution of ROS to the observed antibacterial activity under dark conditions.

For SnO_2, although oxygen vacancies and surface electronic states have also been reported [45], its antibacterial behavior under dark conditions may additionally involve direct surface–bacteria interactions. Direct contact between the oxide surface and bacterial cells can affect cell-envelope integrity and bacterial adhesion, potentially leading to membrane destabilization and loss of cellular viability [46]. Furthermore, physicochemical surface characteristics, including surface roughness, nanometric topography, surface energy, and surface charge, may influence bacterial adhesion and subsequent cell–surface interactions [46,47]. Depending on the physicochemical conditions of the medium, surface charging of SnO_2 may also affect its electrostatic interactions with bacterial cell membranes and contribute to membrane destabilization [47].

In summary, this comparative analysis demonstrates that the antibacterial activity under dark conditions strongly depends on the nature of the exposed surface. The more pronounced inhibition observed for the ZnO/SnO_2 configuration is consistent with a mechanism involving local ROS generation mediated by structural defects in ZnO, independently of any photocatalytic process.

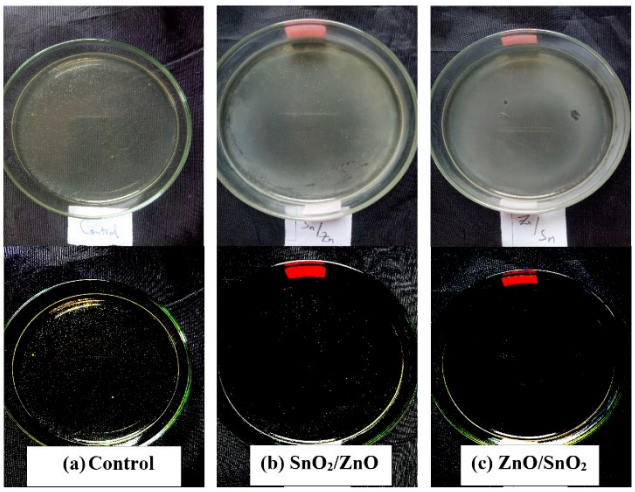

Figure 9. Optical images of Pseudomonas Aeruginosa bacteria growth after 24 h of incubation under effect of ZnO/SnO_2 and SnO_2/ZnO nanofilms.

4. Conclusion

ZnO/SnO_2 and SnO_2/ZnO composite thin films were successfully prepared using the ultrasonic spray pyrolysis technique. XRD investigations confirmed the existence of the hexagonal wurtzite ZnO and tetragonal rutile SnO_2 phases in both composites films. SEM analysis revealed dense, continuous surface with compact nanoscale grains showing good coalescence, while EDX analysis confirmed the presence of Zn, Sn, and O, without detectable impurities. Optical properties measurements showed high transparency in the visible range and strong UV absorption, consistent with the wide bandgap nature of the constituent oxides. The composite thin films exhibited significantly improved photocatalytic, sonocatalytic and antibacterial performance compared with the corresponding individual components, over pure components due to efficient heterojunction charge separation and reactive oxygen species generation with the magnitude of the enhancement depending on the stacking sequence. In particular, ZnO/SnO_2 showed superior photocatalytic and antibacterial performance, whereas SnO_2/ZnO exhibited higher sonocatalytic activity. These differences indicate that the deposition sequence plays an important role in determining the functional performance of the ZnO/SnO_2 heterostructures. The observed enhancement may be associated with interfacial interactions between ZnO and SnO_2 and with improved charge-transfer and reactive-species processes; however, these mechanistic aspects should be considered as proposed interpretations rather than directly verified conclusions. Overall, the results demonstrate that controlling the stacking sequence of ZnO/SnO_2 and SnO_2/ZnO thin-film heterostructures is an effective approach for tuning their photocatalytic, sonocatalytic, and antibacterial properties.

Acknowledgment

Please provide Acknowledgment especially Funder of Research as guided in Section 11.19 (https://journal.bcrec.id/index.php/bcrec/pages/view/authorguide) .

CRediT Author Statement

Author Contributions: Please provide Credit Authors Statement as guided in Section 11.13 (https://journal.bcrec.id/index.php/bcrec/pages/view/authorguide) . All authors have read and agreed to the published version of the manuscript.

References

[1] Elias, Md., Alam, R., Khatun, S., Swapon Hossain, Md., Shaheen Shah, S., Abdul Aziz, Md., Nizam Uddin, Md., Awlad Hossain, M. (2025). Hydrothermal synthesis of carboxylated functionalized jute stick carbon and reduced graphene oxide based ZnO nanocomposite photocatalysts: A comparative study. *Journal of Industrial and Engineering Chemistry*, 143, 424–436. DOI: 10.1016/j.jiec.2024.08.049

[2] Mandal, S.K., Dutta, K., Pal, S., Mandal, S., Naskar, A., Pal, P.K., Bhattacharya, T.S., Singha, A., Saikh, R., De, S., Jana, D. (2019). Engineering of ZnO/rGO nanocomposite photocatalyst towards rapid degradation of toxic dyes. *Materials Chemistry and Physics*, 223, 456–465. DOI: 10.1016/j.matchemphys.2018.11.002

[3] Wang, L.L., Kang, L.P., Wang, H.Y., Chen, Z.P., Li, X.J. (2016). Capacitive humidity sensitivity of SnO 2:Sn thin film grown on silicon nanoporous pillar array. *Sensors and Actuators B: Chemical*, 229, 513–519. DOI: 10.1016/j.snb.2016.02.025

[4] Kavan, L. (2024). Electrochemistry and band structure of semiconductors (TiO2, SnO2, ZnO): Avoiding pitfalls and textbook errors. *Journal of Solid State Electrochemistry*, 28(3–4), 829–845. 10.1007/s10008-023-05770-w

[5] Bousmaha, M., Bezzerrouk, M.A., Kharroubi, B., Akriche, A., Naceur, R., Hattabi, I., Sandjak-Eddine, K. (2019). Enhanced photocatalysis by depositing ZnO thin film in the inner wall of glass tube. *Optik*, 183, 727–731. DOI: 10.1016/j.ijleo.2019.02.111

[6] Sial, M.A.Z.G., Iqbal, M., Siddique, Z., Nadeem, M.A., Ishaq, M., Iqbal, A. (2017). Synthesis and time-resolved photoluminescence of SnO2 nanorods. *Journal of Molecular Structure*, 1144, 355–359. DOI: 10.1016/j.molstruc.2017.05.067

[7] Derri, A., Guezzoul, M., Mokadem, A., Ouerdane, A., Bensassi, K.B., Bouslama, M., Kharoubi, B., Hameurlaine, E. (2023). Insight into the photoluminescence and morphological characteristics of transition metals (TM = Mn, Ni, Co, Cu)-doped ZnO semiconductor: a comparative study. *Optical Materials*, 145, 114467. DOI: 10.1016/j.optmat.2023.114467

[8] Kharroubi, B., Bousmaha, M., Bezzerrouk, M. A., Akriche, A., Naceur, R., Guezzoul, M., Bensassi, K.B., Zahafi, K., Zoukel, A., Abdelkrim, M., Bedrouni, M., Bouslama, M. (2022). Photocatalytic efficiency of undoped and Cu-doped ZnO thin films coated inside transparent glass tube as one-piece photoreactor. *Applied Surface Science*, 601, 154121. DOI: 10.1016/j.apsusc.2022.154121

[9] Bousmaha, M., Kharroubi, B., Bezzerrouk, M. A., Pignon, B., Medjadi, R., Boutiche, M., Akriche, A., Naceur, R., Sahnoune, N., Abdellah, F., Benaraba, R. (2024). Efficient removal of amoxicillin and methyl orange with antibacterial activity assessment via nanostructured ZnO coatings synthesized by ultrasonic spray pyrolysis method. *Ceramics International*, 50(13), 23784–23793. DOI: 10.1016/j.ceramint.2024.04.104

[10] Atay, F., Akyuz, I., Durmaz, D., Kose, S. (2019). Characterization of ZnO-SnO2 oxide systems produced by ultrasonic spray pyrolysis. *Solar Energy*, 193, 666–675. DOI: 10.1016/j.solener.2019.10.012

[11] Bezzerrouk, M.A., Bousmaha, M., Hassan, M., Akriche, A., Kharroubi, B., Naceur, R., Guezzoul, M. (2021). Enhanced methylene blue removal efficiency of SnO2 thin film using sono-photocatalytic processes. *Optical Materials*, 117, 111116. DOI: 10.1016/j.optmat.2021.111116

[12] Firooz, A.A., Mahjoub, A.R., Khodadadi, A.A. (2008). Preparation of SnO2 nanoparticles and nanorods by using a hydrothermal method at low temperature. *Materials Letters*, 62(12–13), 1789–1792. DOI: 10.1016/j.matlet.2007.10.004

[13] Kong, J., Deng, H., Yang, P., Chu, J. (2009). Synthesis and properties of pure and antimony-doped tin dioxide thin films fabricated by sol–gel technique on silicon wafer. *Materials Chemistry and Physics*, 114(2–3), 854–859. DOI: 10.1016/j.matchemphys.2008.10.049

[14] Alsulami, A., Alsalme, A. (2025). Facile synthesis and characterization of the innovative CrVO4 thin films grown by nebulizer spray pyrolysis. *Physica B: Condensed Matter*, 715, 417546. DOI: 10.1016/j.physb.2025.417546

[15] Shikoh, A.S., Paek, S., Polyakov, A.Y., Smirnov, N.B., Shchemerov, I.V., Saranin, D.S., Didenko, S.I., Ahmad, Z., Touati, F., Nazeeruddin, M.K. (2020). Assessing mobile ions contributions to admittance spectra and current-voltage characteristics of 3D and 2D/3D perovskite solar cells. *Solar Energy Materials and Solar Cells*, 215, 110670. DOI: 10.1016/j.solmat.2020.110670

[16] El Fidha, G., Bitri, N., Llobet, E. (2026). Boosting photocatalytic efficiency through Ni–Co co-doped ZnO thin films fabricated by spray pyrolysis. *Physica B: Condensed Matter*, 724, 418187. DOI: 10.1016/j.physb.2025.418187

[17] Srujana, B.S., Prakash, A., Chattopadhyay, S., M.G., M. (2023). Zirconium doped zinc oxide thin films grown by spray pyrolysis technique for TCO applications. *Materials Today Communications*, 37, 107476. DOI: 10.1016/j.mtcomm.2023.107476

[18] Ankam, V., G, L., Y, V., & P, N. (2024). Structural, morphological and optical studies of various substrate temperatures of ZnO thin films by spray pyrolysis. *International Journal of Physics and Applications*, 6(2), 102–107. DOI: 10.33545/26647575.2024.v6.i2b.107

[19] Bezzerrouk, M.A., Akriche, A., Kharroubi, B., Giovannelli, F., Zaghrioui, M., Pignon, B., Naceur, R., Bousmaha, M. (2025). Effect of Sr doping on microstructure, morphology, photoluminescence, optical properties and photocatalytic performance of SnO2 thin films. *Optical Materials*, 167, 117292. DOI: 10.1016/j.optmat.2025.117292

[20] Lagariya, M., Modi, M., Dadhich, H., Gal, M., Gadani, K., Solanki, P.S., Shah, N.A. (2020). Studies on structural and electrical behaviors of chemically grown ZnO/SnO2 nanocomposites. *Physica B: Condensed Matter*, 577, 411774. DOI: 10.1016/j.physb.2019.411774

[21] Li, X., Zhou, L., Zhao, S., Ding, H., Cao, H., Fang, Z., Jiang, F., Li, H., Liu, Y., Zhu, Y. (2023). Reduced graphite oxide wrapped ZnO-SnO2 hollow nanospheres with as anodes for hybrid high energy density supercapacitors. *Diamond and Related Materials*, 136, 110076. DOI: 10.1016/j.diamond.2023.110076

[22] Riahi, I., Khalfallah, B., Chaabouni, F. (2021). Effect of deposition time on the photocatalytic activity of sputtered mixed ZnO–SnO2 thin films under visible light irradiation. Solid State Communications, 340, 114487. DOI: 10.1016/j.ssc.2021.114487

[23] Mimouni, R., Askri, B., Larbi, T., Amlouk, M., Meftah, A. (2020). Photocatalytic degradation and photo-generated hydrophilicity of Methylene Blue over ZnO/ZnCr2O4 nanocomposite under stimulated UV light irradiation. *Inorganic Chemistry Communications*, 115, 107889. DOI: 10.1016/j.inoche.2020.107889

[24] Paniagua-Méndez, J., Ramírez-Sandoval, S.L., Reyes-Uribe, E., Contreras-García, M.E. (2024). Photocatalytic activity and biocide effect of nanostructured SnO2/ZnO/TiO2 thin film heterostructure obtained by sol-gel spin coating technique. *Ceramics International*, 50(18), 34421–34430. DOI: 10.1016/j.ceramint.2024.06.261

[25] Kappadan, S., Thomas, S., Kalarikkal, N. (2020). BaTiO3/ZnO heterostructured photocatalyst with improved efficiency in dye degradation. *Materials Chemistry and Physics*, 255, 123583. DOI: 10.1016/j.matchemphys.2020.123583

[26] Rogé, V., Didierjean, J., Crêpellière, J., Arl, D., Michel, M., Fechete, I., Dinia, A., Lenoble, D. (2020). Tuneable Functionalization of Glass Fibre Membranes with ZnO/SnO2 Heterostructures for Photocatalytic Water Treatment: Effect of SnO2 Coverage Rate on the Photocatalytic Degradation of Organics. *Catalysts*, 10(7), 733. DOI: 10.3390/catal10070733

[27] Dharmana, G., Nadikatla, S.K., Gurugubelli, T. R., Viswanadham, B. (2024). Enhanced Photo-Catalytic Degradation of MB Dye over Hydrothermal Grown-Up of ZnO/SnO2 Catalyst. *Journal of Chemistry*, 2024(1). DOI: 10.1155/2024/9135923

[28] Alfaro Cruz, M.R., Saldaña-Ramírez, A., Juárez-Ramírez, I., Torres-Martínez, L.M. (2023). Development of SnO2–ZnO thin films as a photocatalyst for obtaining alternative fuels through photocatalytic reactions. *Solid State Sciences*, 137, 107112. DOI: 10.1016/j.solidstatesciences.2023.107112

[29] Zhang, H., Zong, R., Zhu, Y. (2009). Photocorrosion Inhibition and Photoactivity Enhancement for Zinc Oxide via Hybridization with Monolayer Polyaniline. The Journal of Physical Chemistry C, 113(11), 4605–4611. DOI: 10.1021/jp810748u

[30] Hamrouni, A., Moussa, N., Parrino, F., Di Paola, A., Houas, A., Palmisano, L. (2014). Sol–gel synthesis and photocatalytic activity of ZnO–SnO2 nanocomposites. Journal of Molecular Catalysis A: Chemical, 390, 133–141. DOI: 10.1016/j.molcata.2014.03.018

[31] Zhang, J., Yu, X.C., Nie, Z.W., Guo, M.C., Liu, J.H., Wang, L.P. (2017). Preparation of ZnO/SnO2 Composite Nanometer Photocatalyst and Photocatalytic Treatment of Marine Diesel Pollution. *IOP Conference Series: Materials Science and Engineering*, 281, 012015. DOI: 10.1088/1757-899x/281/1/012015

[32] Zankat, A., Gadani, K., Vadgama, V., Udeshi, B., Gal, M., Solanki, S., Vaishnani, A., Shrimali, V.G., Solanki, P.S., Shah, N.A., Pandya, D.D. (2021). Frequency and temperature dependent electrical properties of ZnO–SnO2 nanocomposites. *Physica B: Condensed Matter*, 617, 413140. DOI: 10.1016/j.physb.2021.413140

[33] Motsoeneng, R.G., Swart, H.C., Motaung, D.E. (2023). The influence of Fe loading on the optical and gas sensing characteristics of SnO2/ZnO heterostructures. *Physica B: Condensed Matter*, 668, 415256. DOI: 10.1016/j.physb.2023.415256

[34] Bedrouni, M., Kharroubi, B., Ouerdane, A., Bouslama, M., Guezzoul, M., Caudano, Y., Bensassi, K.B., Bousmaha, M., Bezzerrouk, M.A., Mokadem, A., Abdelkrim, M. (2021). Effect of indium incorporation, stimulated by UHV treatment, on the chemical, optical and electronic properties of ZnO thin film. *Optical Materials*, 111, 110560. DOI: 10.1016/j.optmat.2020.110560

[35] Caglar, M., Atar, K.C. (2012). Effect of both deposition temperature and indium doping on the properties of sol–gel dip–coated SnO2 films. *Spectrochimica Acta Part A: Molecular and Biomolecular Spectroscopy*, 96, 882–888. DOI: 10.1016/j.saa.2012.07.108

[36] Rao, A.D., Bairy, R., Kulkarni, S.D., Gummagol, N. (2026). Influence of deposition time on optoelectronic properties of Ni-doped SnO2 thin films for NLO device applications. *Physica B: Condensed Matter*, 723, 418112. DOI: 10.1016/j.physb.2025.418112

[37] Yadav, T.P., Teli, S.B., Salunkhe, Shilpa. Y., Deshmukh, S.M., Garadkar, K.M. (2025). Evaluation of photocatalytic and antibacterial properties of SnO2-ZnO nanocomposites developed by Calotropis gigantea leaf extract. *Next Materials*, 9, 101197. DOI: 10.1016/j.nxmate.2025.101197

[38] Sefardjella, H., Boudjema, B., Kabir, A., Schmerber, G. (2013). Structural and photoluminescence properties of SnO2 obtained by thermal oxidation of evaporated Sn thin films. *Current Applied Physics*, 13(9), 1971–1974. DOI: 10.1016/j.cap.2013.08.017

[39] Ali, A.M., Ismail, A.A., Najmy, R., Al-Hajry, A. (2014). Preparation and characterization of ZnO–SiO2 thin films as highly efficient photocatalyst. *Journal of Photochemistry and Photobiology A: Chemistry*, 275, 37–46. DOI: 10.1016/j.jphotochem.2013.11.002

[40] Torres Martínez, D.Y., Castanedo Pérez, R., Torres Delgado, G., Zelaya Ángel, O. (2012). Structural, morphological, optical and photocatalytic characterization of ZnO–SnO2 thin films prepared by the sol–gel technique. *Journal of Photochemistry and Photobiology A: Chemistry*, 235, 49–55. DOI: 10.1016/j.jphotochem.2012.03.009

[41] Sin, J.-C., Lam, S.-M., Lee, K.-T., Mohamed, A.R. (2014). Preparation of rare earth-doped ZnO hierarchical micro/nanospheres and their enhanced photocatalytic activity under visible light irradiation. *Ceramics International*, 40(4), 5431–5440. DOI: 10.1016/j.ceramint.2013.10.128

[42] Tashakkori Masuleh, M., Hasheminiasari, M., Ashiri, R. (2025). Enhanced photocatalytic efficiency of eco-friendly synthesized ZnO for rapid full degradation of methylene blue dye. *Materials Advances*, 6(8), 2611–2621. DOI: 10.1039/d5ma00026b

[43] Biswas, A., Kar, U., Jana, N.R. (2022). Cytotoxicity of ZnO nanoparticles under dark conditions via oxygen vacancy dependent reactive oxygen species generation. *Physical Chemistry Chemical Physics*, 24(22), 13965–13975. DOI: 10.1039/d2cp00301e

[44] Imlay, J. A. (2003). Pathways of Oxidative Damage. Annual Review of Microbiology, 57(1), 395–418. DOI: 10.1146/annurev.micro.57.030502.090938

[45] Xiong, Y., Lin, Y., Wang, X., Zhao, Y., Tian, J. (2022). Defect engineering on SnO2 nanomaterials for enhanced gas sensing performances. *Advanced Powder Materials*, 1(3), 100033. DOI: 10.1016/j.apmate.2022.02.001

[46] Ivanova, E.P., Hasan, J., Webb, H.K., Truong, V.K., Watson, G.S., Watson, J.A., Baulin, V.A., Pogodin, S., Wang, J.Y., Tobin, M.J., Löbbe, C., Crawford, R.J. (2012). Natural Bactericidal Surfaces: Mechanical Rupture of Pseudomonas aeruginosa Cells by Cicada Wings. *Small*, 8(16), 2489–2494. DOI: 10.1002/smll.201200528

[47] Chávez-Calderón, A., Paraguay-Delgado, F., Orrantia-Borunda, E., Luna-Velasco, A. (2016). Size effect of SnO 2 nanoparticles on bacteria toxicity and their membrane damage. *Chemosphere*, 165, 33–40. DOI: 10.1016/j.chemosphere.2016.09.003.